Iodine–Iodine Cooperation Enables Metal-Free C–N Bond-Forming Electrocatalysis via Isolable Iodanyl Radicals

Brandon L. Frey,[†] Matthew T. Figgins,[†] Gerard P. Van Trieste III,[†] Raanan Carmieli,[#] and David C. Powers[†,*]

[†] Department of Chemistry, Texas A&M University, College Station, TX 77843, USA

[#] Department of Chemical Research Support, Weizmann Institute of Science, Rehovot, Israel

*powers@chem.tamu.edu

Abstract Small molecule redox mediators convey interfacial electron transfer events into bulk solution and can enable diverse substrate activation mechanisms in synthetic electrocatalysis. Here we report that 1,2-diiodo-4,5-dimethoxybenzene (**1a**) is an efficient electrocatalyst for C–H/E–H coupling that operates at as low as 0.5 mol% catalyst loading. Spectroscopic, crystallographic, and computational results indicate a critical role for a three-electron I–I bonding interaction in stabilizing an iodanyl radical intermediate (*i.e.*, formally I(II) species). As a result, **1a** operates at more than 100 mV lower potential than related monoiodide catalysts, which results in improved product yield, higher Faradaic efficiency, and expanded substrate scope. The isolated iodanyl radical is chemically competent in C-N bond formation. These results represent the first examples of substrate functionalization at a well-defined I(II) derivative and *bona fide* iodanyl radical catalysis and demonstrate one-electron pathways as a mechanistic alternative to canonical two-electron hypervalent iodine mechanisms. The observation establishes I–I redox cooperation as a new design concept for the development of metal-free redox mediators.

The development of indirect electrochemical mediators, which are redox-active small molecules that participate in well-defined interfacial electron transfer (ET) and convey the resulting electron or hole equivalents into the bulk phase, has powerfully enabled the development of organic electrocatalysis.[1, 2] Identification of new mediators that engage in diverse modes of substrate activation and that can aggregate the multiple electron equivalents needed for the two-electron bond-making processes in organic synthesis, provide the opportunity to marry interfacial electron transfer with an array of synthetic transformations. Hypervalent iodine compounds are a broadly deployed class of chemoselective oxidants,[3-7] and the potential to utilize aryl iodides as indirect electrochemical mediators (*i.e.*, electrocatalysts) has garnered significant attention (Figure 1).[8-12] Thus far, high catalyst loading, limited substrate scope, and the high onset potential for anodic oxidation has stymied development of hypervalent iodine electrocatalysis and largely limited application of these mediators to *ex cell* transformations.

Organic hypervalent I(III) and I(V) reagents are commonly encountered oxidants in fine-chemical synthesis that operate via selective two-electron oxidation-reduction processes. Recently, transient iodanyl radicals (*i.e.*, formally I(II) species) have been proposed as intermediates in the photochemistry of I(III) compounds[13] and as intermediates in aerobic and electrochemical syntheses of I(III) derivatives.[11, 13-15] For example, in 2020 we reported an electrochemical C–H / N–H coupling catalyzed by iodoanisole that was proposed to proceed via carboxylate-stabilized iodanyl radicals.[11] While increasingly invoked, the complete lack of isolable organic I(II) compounds has prevented interrogation of potential reactions of these open-shell species towards substrates.

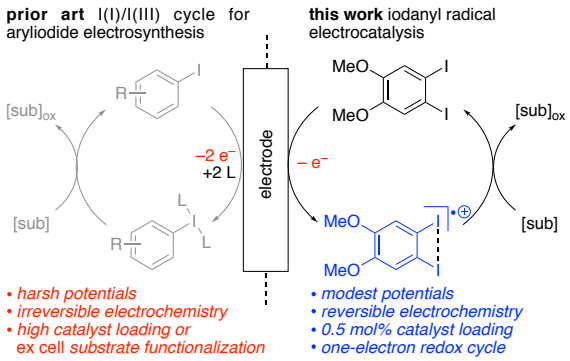

Figure 1. Two-electron vs. one-electron hypervalent iodine catalysis.

Inspired by 1) the reversible electrochemistry of veratrole derivatives (*i.e.*, dimethoxybenzenes)[16] and 2) the delocalized I–I interactions in σ-aromatic $C_6I_6^{2+}$,[17] we identified 1,2-diiodo-4,5-dimethoxybenzene (**1a**) as a highly efficient and robust catalyst for a suite of C–H functionalization reactions at catalyst loadings as low as 0.5 mol%. Detailed electrochemical and *in situ* spectroscopic experiments indicate that these reactions are mediated by the iodanyl radical generated by one-electron oxidation of **1a**. Synthesis and isolation of the incipient iodanyl radical (**1a**$^+$) enabled complete spectroscopic and crystallographic characterization. The isolated iodanyl radical is chemically competent as an intermediate in C–H functionalization. These observations raise the specter of I(I/II) catalytic cycle involving direct substrate engagement by an iodanyl radical, which contrasts with traditional two-electron hypervalent iodine cycles.

We initiated our studies by examining the impact of aryliodide structure on the electrochemical C–N coupling of biarylamide **2** to afford the corresponding carbazole (**3**). Previous attempts to lower the catalyst loading from 25 mol% (optimized condition with 4-iodoanisole (**1b**) as catalyst) resulted in significantly decreased reaction efficiency: At 5 mol% **1b** only 30% carbazole was produced and lowering further to 0.5 mol% catalyst loading resulted in 6% carbazole formation (Figure 2, Table S1). 4-Iodo-1,2-dimethoxybenzene (**1c**), which features a second methoxy substituent, displays significantly increased electrochemical reversibility and decreased the onset

potential for oxidation, but poor catalytic activity (8% yield in cyclization of **2**). 1,2-Diiodo-4-methoxybenzene (**1d**), which features a second iodine substituent, displays poorer electrochemical reversibility and neither lowered the observed $E_{1/2}$ nor resulted in improved catalysis. In contrast, 1,2-diiodo-4,5-dimethoxybenzene (**1a**), which features two iodine and two methoxy substituents, displays a reversible wave at $E_{1/2}$=1.13 V vs. Fc^+/Fc, a 200 mV lower E_{pa} than **1b**, and is a highly efficient catalyst. With **1a**, the catalyst loading could be lowered to 0.5 mol% with no loss of yield or FE (*i.e.*, 92% yield, 73% FE, Figure 2a). The relative positions of the iodine substituents are crucial to catalytic efficiency: 1,4-Diiodo-2,5-dimethoxybenzene (**1e**) displays $E_{1/2}$ = 1.09 but is an inefficient C–N coupling catalyst (8% yield in cyclization of **2**). Other 1,2-dimethoxybenzene derivatives (**1f-1h**) and electron-rich arenes were examined and were generally poorly efficient catalysts (Figure 2a and S1).

The nature of the electrochemical processes observed of **1a** was analyzed by examining the relative cathodic (I_{PC}) and anodic currents (I_{PA}) as well as the separation of the oxidation and reduction peaks (ΔE_p) in CVs of **1a**. In these experiments, CVs were obtained for hfip solutions of **1a** with [TBA]PF_6 as electrolyte and a scan rate of 0.1 V/s. Under these conditions, the I_{pc}/I_{pa} ratio, which provides a measure of electrochemical reversibility and thus the stability of the electrochemically generated species, was 0.83 (*c.f.* under these conditions, I_{pa}/I_{pc} = 1.0 for ferrocene; Figure S2, Table S2). ΔE_p for **1a** was measured to be 174 mV; for comparison, ΔE_p for ferrocene was 187 mV under these conditions (Figure S2, Table S2). The significant deviation from ideality (*i.e.*, ΔE_p = 59 mV) likely results from slow electron transfer kinetics under the reaction conditions.[18, 19] Further support for a one-electron event was obtained by integration of the square-wave voltammetry data of **1a** and Fc, which are similar (Figure S3).[20] Analyses of other veratrole derivatives are summarized in Figures S4 and Table S3.

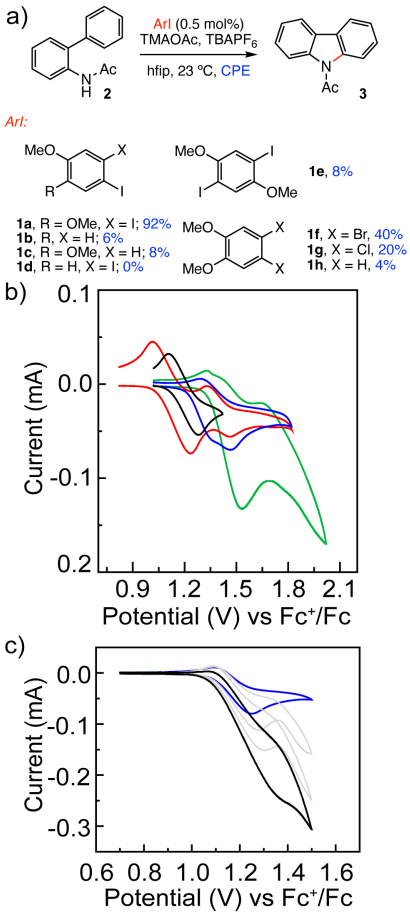

Figure 2. a) Impact of catalyst structure on cyclization efficiency. Conditions: CPE at the E_{pa} of **1** determined by CV in an undivided cell with a glassy carbon anode, a platinum-plated cathode, and a Ag^{+}/Ag reference electrode. a) CVs of **1a** (—), **1b** (—), **1c** (—), and **1d** (—) measured of **1** (5 mM) in 0.2 M $TBAPF_6$/hfip at 0.1 V/s. b) CVs of **1a** (5 mM) with 35.5 mM [TMA]OAc in 0.2 M $TBAPF_6$/hfip at 0.1 V/s varying biarylamide **2** loading 0.0 mM (—), 1.9, 6.1, and 12 mM (—).

To gain insight into the impact of substrate (**2**) and acetate, which is required for efficient C–N coupling, CVs were measured as a function of the concentration of these species. Addition of [TMA]OAc to CV solutions of **1a** resulted in increased oxidative current and partial loss of reversibility (Figure S5, I_{pc}/I_{pa} = 0.52 with 35.5 mM [TMA]OAc). We previously interpreted similar observations in CVs of 4-iodoanisole **1b** as consistent with acetate binding to an anodically generated iodanyl radical.[11] In the case of **1a**, reversibility can be recaptured at higher scan rates, as the rate of reduction outcompetes the electron transfer with added acetate (Figure S6). Addition

of substrate **2** to CVs of **1a** does not affect the reversible wave observed for **1a** (a new peak at E_{pa}=1.55 V vs. Fc^+/Fc grows in (Figure S7), a result of direct substrate oxidation (Figure S8)). Addition of both **2** and [TMA]OAc to CVs of **1a** resulted in the observation of catalytic current where reversibility could not be regained regardless of scan rate, indicative of rapid catalytic turn over (Figure 2b).

Given the single-electron inventory indicated by CV analysis, we were interested in the possibility that substrate activation may arise from one-electron oxidation of **1a** without subsequent generation of an I(III) intermediate. Constant potential electrolysis (CPE) of an hfip solution of **1a** (0.2 M $[TBA]PF_6$ added as electrolyte) in the absence of either acetate or **2** resulted in a drastic color change from colorless to dark blue (Figure 3). The UV-vis spectrum of this solution, acquired *in situ* via spectroelectrochemistry or *ex situ* following the cessation of electrolysis, displayed a broad low-energy absorbance centered at 613 nm (Figure 3a (—), Figure S9 and S10). Acquisition of spectra periodically during the electrolysis reveal the presence of an isosbestic point at 380 nm, which indicates the lack of an intermediate in the anodic oxidation of **1a**. The observed UV-vis spectrum is consistent with reported veratrole-derived radical cations[16, 21, 22] (red shifted due to the heavy atom effect of two iodides). Time-Dependent Density Functional Theory (TD-DFT) computations reproduce the low-energy feature in the spectrum of $\mathbf{1a}^+$ (λ_{max}= 645 nm, Figure 3a (—, —)).[23] The largest orbital contribution to this transition is β-HOMO(-2) to β-LUMO , which is primarily π-to-π* with significant contribution from the in-phase combination of I–centered p-orbitals.

Two experiments were carried out to confirm the blue solution represented single-electron oxidation of **1a**. First, addition of one equivalent of *N,N*-dimethylaniline results in the consumption $\mathbf{1a}^+$ (with concurrent regeneration of **1a**) and the quantitative evolution of the *N,N*-dimethylaniline

radical cation (Figure S11). Second, *in situ* EPR experiments[24] are consistent with one-electron oxidation of **1a** to generate an open-shell species. The resulting spectrum displays narrow spectral width (25 G) that is well-simulated with $2a_I$ = 1.67 G, $2a_H$ = 3.35 G, and $2a_{Me}$ = 0.343 G (Figure 3b). For comparison, under identical *in situ* conditions, neither 4-iodotoluene or 4-bromoanisole provide a spectral signature (Figure S12).

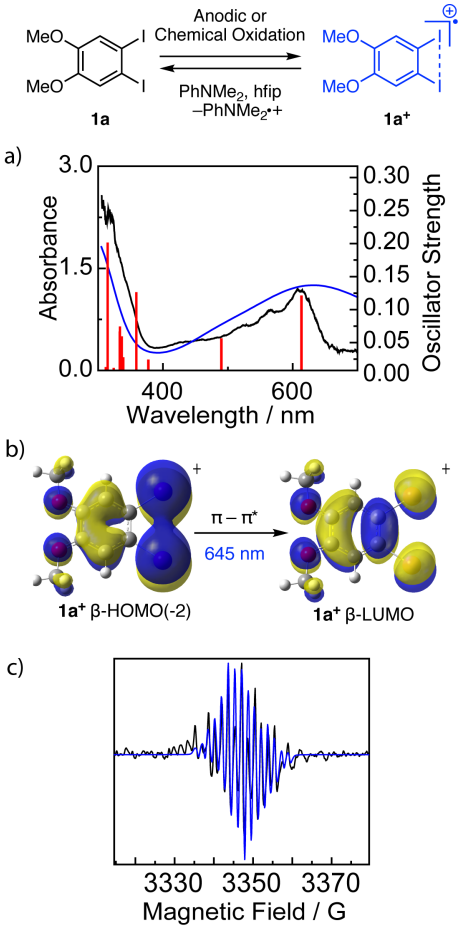

Figure 3. Oxidation of **1a** affords iodanyl radical **1a**$^+$. Oxidation: 5 mM **1a** in a 0.2 M $TBAPF_6$/hfip solution, CPE 1.22 V vs. Fc^+/Fc; or, 0.5 equivalents PIFA, $BF_3{\cdot}OEt_2$ in CH_2Cl_2. Reduction: 1.0 equivalent of *N,N*-dimethylaniline in hfip. a) *In situ* UV-vis spectra collected during CPE of 5 mM **1a** (—). TD–DFT absorption spectrum of **1a**$^+$ (—), and electronic configurations of excited states for **1a**$^+$ (—). b) Most significant contributors to the computed transition at 645 nm. c) *In situ* EPR spectra collected during CPE of 1 mM **1a** (—) and simulated spectrum of **1a**$^+$ (—).

To simplify isolation and independent characterization of iodanyl radical **1a**$^+$, we pursued chemical oxidation of **1a** to avoid the use of supporting electrolyte. Treatment of **1a** with 0.5 equivalents of bis(trifluoroacetoxy)iodobenzene (PIFA) and excess $BF_3{\cdot}OEt_2$ in CH_2Cl_2 resulted

in a dark-blue solution that was spectroscopically identical to the electrochemically generated solution (for comparison of UV-vis spectra and solvatochromism, see Figure S13).[25] Dark blue X-ray quality single-crystals of **1a**$^+$ were obtained on prolonged standing of reaction solutions at –22 °C (Figure 4a; solid-state and solution-phase UV-vis of redissolved crystals are collected in Figure S13). X-ray diffraction of the obtained single crystals provided the molecular structure pictured in Figure 4a. The metrical parameters of **1a** are similar to those of **1a**$^+$, with the exception of a marked contraction of the I–I distance from 3.71157(2) in **1a** to 3.6391(7) in **1a**$^+$ (for complete comparison of **1a** and **1a**$^+$, see Figure S14, Table S4-S6). Charge balance in the crystal is maintained by 0.5 $B_2F_6O^{2-}$ dianions per **1a**$^+$(See Table S7 and Figure S15 for refinement details).

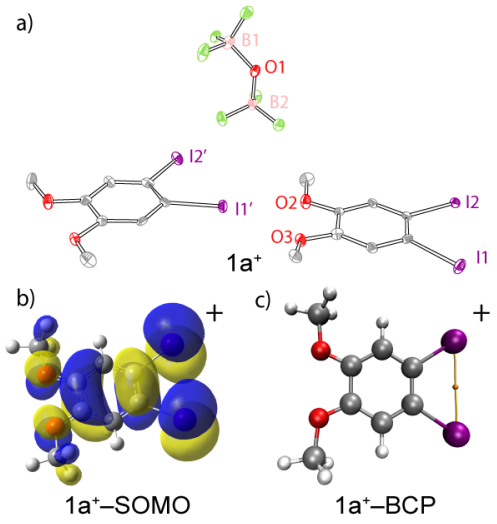

Figure 4. Displacement ellipsoid plot of **1a**$^+$ drawn at 50% probability, H-atoms are omitted for clarity. Selected metrical parameters: C1–I1 = 2.076(6) Å, I1–I2 = 3.6392(7) Å, B1–O1 = 1.513(9) Å, B2–O1 = 1.520(9) Å. b) Computed SOMO of **1a**$^+$. c) Atoms-in-molecules (AIM) analysis indicates an I–I bond critical point (BCP).

DFT optimized structures of **1a** and **1a**$^+$ provide metrics that are in close agreement with those determined by X-ray crystallography (Tables S8 and S9). In particular, the noted contraction of the I–I vector is well described in the computed structures: one-electron oxidation leads to a computed I–I contraction from 3.70 Å for **1a** to 3.65 Å for **1a**$^+$. The singly occupied molecular

orbital (SOMO) of **1a**$^+$ displays predominantly π-character with significant orbital contribution from the iodine atoms (~35% iodine-iodine AO contribution to the SOMO, Figure 4b). We envisioned that the observed I–I contraction may arise from oxidatively induced delocalized 3-electron bonding, which is well-precedented in proximal heavy main-group elements, such as diselenides and disulfides,[26-28] but unknown in hypervalent iodine chemistry. Atoms-in-molecules (AIM) analysis indicates an electron density of $\rho(r)= 0.0123\ e\cdot bohr^{-3}$ and a Laplacian distribution of $\nabla^2\rho(r)=0.0323\ e\cdot bohr^{-5}$ at the I-I bond critical point (BCP) for **1a**$^+$ (Figure 4c). For comparison, no BCP is observed between the I atoms in **1a** (Figure S16). The ρ(r) observed at the BCP of **1a**$^+$ is within the range of values expected for I-I bonds.[29]

Isolation of **1a**$^+$ provided the first opportunity to directly evaluate the reactivity of organic I(II) derivatives in substrate functionalization. Treatment of **1a**$^+$ reactions with biarylamide **2** and [TMA]OAc in hfip resulted in immediate disappearance of the blue color and the evolution of carbazole **3** (35% yield) and quantitative recovery of **1a** (Figure 5a). With demonstration of the chemical competence of iodanyl radical **1a**$^+$ in substrate functionalization and the significantly decreased oxidation potential of **1a** as compared to **1b**, we examined the potential to achieve other C-E bond-forming reactions (Figure 5b). Oxidative dearomatization of **4** was successfully demonstrated with catalyst loading as low as 1 mol% producing 61% product **5**. C(sp^2)-O bond formation can be accomplished from biarylcarboxylic acid **6** to afford **7** under electrocatalytic conditions (5 mol% **1a**) loading.[30] In the absence of **1a** no background oxidation of either **4** or **6** was observed. Additionally, intermolecular benzylic acetoxylation of **8** to generate **9** was accomplished in 74% although higher catalyst loading (25 mol%) was required for high yield. Direct oxidation of **8** for extended reaction times in the absence of catalysts shows greater preference for the benzylic ketone product (40%) and only 20% acetoxylated product **9**.

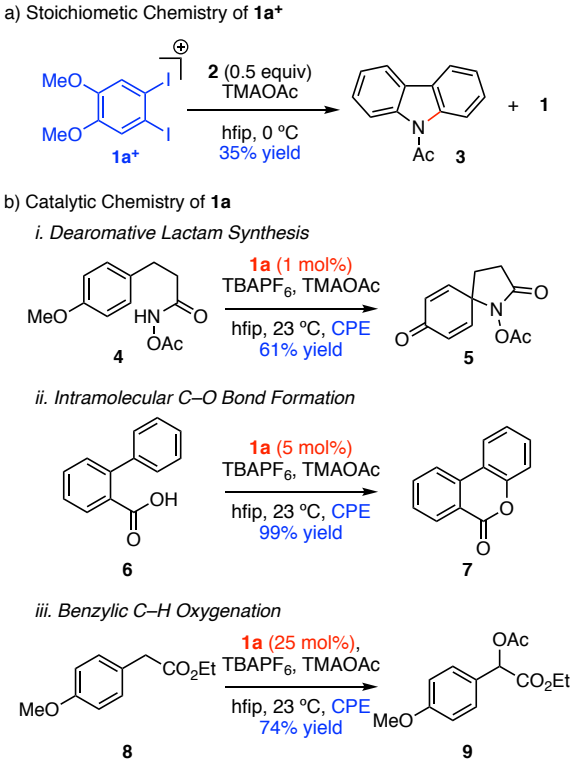

Figure 5. a) Iodanyl radical promotes conversion of **2** to **3**. b) Diiodide **1** catalyzes i) oxidative dearomatization, ii) lactone cyclization, and iii) benzylic acetoxylation. CPE at 1.22 V vs. Fc^+/Fc. Reactions were optimized to the lowest catalyst loading without suffering current density (>1.0 mA).

In conclusion, the critical role of polymethoxy and ortho-diiodide functional groups were shown to have significantly improved substrate scope and catalytic efficiency working at as low as 0.5 mol% loading. Multiple spectroscopic techniques were used that suggest evidence of a three-electron two-centered I–I bond. This is to the best of our knowledge is the first example of selective I(II) synthesis, characterization, and direct reactivity studies. We hypothesize these mechanistic insights herein support I(II) species as competent oxidants rather than just intermediates in multielectron oxidation process and expand the reactivity modes of iodine-based oxidants.

Acknowledgement

The authors acknowledge the National Institutes of Health (R35GM138114) and the Welch Foundation (A-1907) for support. Exploratory studies of the electrochemistry of 1a were supported by the National Science Foundation (CAREER 1848135). Structure determinations were collected at NSF′s ChemMatCARS Sector 15, which is principally supported by the Divisions of Chemistry (CHE) and Materials Research (DMR), NSF, under Grant NSF/CHE-1834750. Use of the Advanced Photon Source, an Office of Science User Facility operated for the U.S. DOE Office of Science by Argonne National Laboratory, was supported by the U.S. DOE under Contract DE-AC02-06CH11357. The computational work was completed with resources provided by the Texas A&M University High Performance Research Computing (HPRC) center.

References

1. Francke, R.; Little, R. D., Redox catalysis in organic electrosynthesis: basic principles and recent developments. *Chem. Soc. Rev.* **2014,** *43*, 2492–2521.
2. Yan, M.; Kawamata, Y.; Baran, P. S., Synthetic Organic Electrochemical Methods Since 2000: On the Verge of a Renaissance. *Chem. Rev.* **2017,** *117*, 13230–13319.
3. Brand, J. P.; González, D. F.; Nicolai, S.; Waser, J., Benziodoxole-based hypervalent iodine reagents for atom-transfer reactions. *Chem. Commun.* **2011,** *47*, 102–115.
4. Charpentier, J.; Früh, N.; Togni, A., Electrophilic Trifluoromethylation by Use of Hypervalent Iodine Reagents. *Chem, Rev,* **2015,** *115*, 650–682.
5. Sousa, E. S. F. C.; Tierno, A. F.; Wengryniuk, S. E., Hypervalent Iodine Reagents in High Valent Transition Metal Chemistry. *Molecules* **2017,** *22,* 780–834.
6. Yoshimura, A.; Yusubov, M. S.; Zhdankin, V. V., Synthetic applications of pseudocyclic hypervalent iodine compounds. *Org. Biomol. Chem.* **2016,** *14*, 4771–4781.
7. Yoshimura, A.; Zhdankin, V. V., Advances in Synthetic Applications of Hypervalent Iodine Compounds. *Chem. Rev.* **2016,** *116*, 3328–3435.
8. Aertker, K.; Rama, R. J.; Opalach, J.; Muñiz, K., Vicinal Difunctionalization of Alkenes under Iodine(III) Catalysis involving Lewis Base Adducts. *Adv. Synth. Catal.* **2017,** *359*, 1290–1294.
9. Fuchigami, T.; Fujita, T., Electrolytic Partial Fluorination of Organic Compounds. 14. The First Electrosynthesis of Hypervalent Iodobenzene Difluoride Derivatives and Its Application to Indirect Anodic gem-Difluorination. *J. Org. Chem,* **1994,** *59*, 7190–7192.
10. Kong, X.; Lin, L.; Chen, X.; Chen, Y.; Wang, W.; Xu, B., Electrochemical Oxidative Syntheses of NH-Sulfoximines, NH-Sulfonimidamides and Dibenzothiazines via Anodically Generated Hypervalent Iodine Intermediates. *ChemSusChem* **2021,** *14*, 3277–3282.
11. Maity, A.; Frey, B. L.; Hoskinson, N. D.; Powers, D. C., Electrocatalytic C–N Coupling via Anodically Generated Hypervalent Iodine Intermediates. *J. Am. Chem. Soc.* **2020,** *142*, 4990–4995.
12. Massignan, L.; Tan, X.; Meyer, T. H.; Kuniyil, R.; Messinis, A. M.; Ackermann, L., C–H Oxygenation Reactions Enabled by Dual Catalysis with Electrogenerated Hypervalent Iodine Species and Ruthenium Complexes. *Angew. Chem, Int. Ed.* **2020,** *59*, 3184–3189.

13. Wang, X.; Studer, A., Iodine(III) Reagents in Radical Chemistry. *Acc. Chem. Res.* **2017,** *50*, 1712–1724.
14. Hyun, S.-M.; Yuan, M.; Maity, A.; Gutierrez, O.; Powers, D. C., The Role of Iodanyl Radicals as Critical Chain Carriers in Aerobic Hypervalent Iodine Chemistry. *Chem* **2019,** *5*, 2388–2404.
15. Habert, L.; Cariou, K., Photoinduced Aerobic Iodoarene-Catalyzed Spirocyclization of N-Oxy-amides to N-Fused Spirolactams. *Angew. Chem. Int. Ed.* **2021,** *60*, 171–175.
16. Huang, J.; Pan, B.; Duan, W.; Wei, X.; Assary, R. S.; Su, L.; Brushett, F. R.; Cheng, L.; Liao, C.; Ferrandon, M. S.; Wang, W.; Zhang, Z.; Burrell, A. K.; Curtiss, L. A.; Shkrob, I. A.; Moore, J. S.; Zhang, L., The lightest organic radical cation for charge storage in redox flow batteries. *Sci. Rep.* **2016,** *6*, 32102–32111.
17. Sagl, D. J.; Martin, J. C., The stable singlet ground state dication of hexaiodobenzene: possibly a sigma-delocalized dication. *J. Am. Chem. Soc.* **1988,** *110*, 5827–5833.
18. Sandford, C.; Edwards, M. A.; Klunder, K. J.; Hickey, D. P.; Li, M.; Barman, K.; Sigman, M. S.; White, H. S.; Minteer, S. D., A synthetic chemist's guide to electroanalytical tools for studying reaction mechanisms. *Chem. Sci.* **2019,** *10*, 6404–6422.
19. Costentin, C.; Savéant, J.-M., Multielectron, Multistep Molecular Catalysis of Electrochemical Reactions: Benchmarking of Homogeneous Catalysts. *ChemElectroChem* **2014,** *1*, 1226–1236.
20. The significant deviation from an ideally reversible system prevents traditional electroanalytical analysis of 1a via the Randles-Sevcik equation making direct calculation of the number of electrons transferred unreliable.
21. Horibe, T.; Ohmura, S.; Ishihara, K., Structure and Reactivity of Aromatic Radical Cations Generated by FeCl3. *J. Am. Chem. Soc.* **2019,** *141*, 1877–1881.
22. Rathore, R.; Wadumethrige, S. H., Highly robust cation radical salts: Aromatic oxidants from cycloannulated aromatic donors. *Journal of Photochemistry and Photobiology A: Chemistry* **2019,** *382*, 111882.
23. All optimizations were performed at the B3LYP-D3BJ/BS1 (BS1 defined in the Computational Methods Details in the SI) level of theory. TD–DFT single points were performed on the optimized geometries to calculate the first 30 excitations.
24. Toybenshlak, M.; Carmieli, R., A New and Robust Method for In-situ EPR Electrochemistry. *Isr. J. Chem.* **2019,** *59*, 1020–1026.
25. Other one electron oxidants including Fe(III), Ce(IV), and nitrosium salts produced indistinguishable UV-vis spectra upon oxidation of **1a** however were unsuccessful in producing single crystals.
26. Yang, W.; Zhang, L.; Xiao, D.; Feng, R.; Wang, W.; Pan, S.; Zhao, Y.; Zhao, L.; Frenking, G.; Wang, X., A diradical based on odd-electron σ-bonds. *Nat. Commun.* **2020,** *11*, 3441–3449.
27. Zhang, S.; Wang, X.; Su, Y.; Qiu, Y.; Zhang, Z.; Wang, X., Isolation and reversible dimerization of a selenium–selenium three-electron σ-bond. *Nat. Commun.* **2014,** *5*, 4127–4134.
28. Zhang, S.; Wang, X.; Sui, Y.; Wang, X., Odd-Electron-Bonded Sulfur Radical Cations: X-ray Structural Evidence of a Sulfur–Sulfur Three-Electron σ-Bond. *J. Am. Chem. Soc.* **2014,** *136*, 14666–14669.
29. Bartashevich, E. V.; Yushina, I. D.; Stash, A. I.; Tsirelson, V. G., Halogen Bonding and Other Iodine Interactions in Crystals of Dihydrothiazolo(oxazino)quinolinium Oligoiodides from the Electron-Density Viewpoint. *Cryst. Growth Des.* **2014,** *14*, 5674–5684.
30. Togo, H.; Muraki, T.; Yokoyama, M., Remote functionalization (1): Synthesis of γ- and δ-lactones from aromatic carboxylic acids. *Tetrahedron Lett.* **1995,** *36*, 7089–7092.